Conventional isotropic *s*-wave superconductivity with strong electron-phonon coupling in $Sc_5Rh_6Sn_{18}$

Manuel Feig,[1,2] Walter Schnelle,[2] Alexander Maisuradze,[3,4,5] Alfred Amon,[2] Christopher Baines,[4] Michael Nicklas,[2] Silvia Seiro,[6] Ludovic Howald,[4] Rustem Khasanov,[4] Andreas Leithe-Jasper,[2] and Roman Gumeniuk[1,*]

[1]*Institut für Experimentelle Physik, TU Bergakademie Freiberg, Leipziger Straße 23, D-09596 Freiberg, Germany*
[2]*Max-Planck-Institut für Chemische Physik fester Stoffe, Nöthnitzer Straße 40, D-01187 Dresden, Germany*
[3]*Physik-Institut der Universität Zürich, Winterthurerstrasse 190, CH-8057 Zürich, Switzerland*
[4]*Laboratory for Muon Spin Spectroscopy, Paul Scherrer Institut, CH-5232 Villigen PSI, Switzerland*
[5]*Department of Physics, Tbilisi State University, Chavchavadze 3, GE-0128 Tbilisi, Georgia*
[6]*Leibniz IFW Dresden, Helmholtzstraße 20, D-01069 Dresden, Germany*

(Received 31 January 2020; revised 29 May 2020; accepted 23 June 2020; published 7 July 2020)

$Sc_5Rh_6Sn_{18}$ is a diamagnetic metallic compound (space group: $I4_1/acd$, $a \approx 13.5$ Å, $c \approx 27.1$ Å) which becomes superconducting (sc) at $T_c = 5.15$ K. The sc state was studied on single-crystal samples by temperature- and field-dependent electrical resistivity, specific heat, and muon-spin rotation (μSR) spectroscopy. No anisotropy of the upper critical field $B_{c2} = 7.75$ T is observed. Analyses of specific heat indicate enhanced values of the jump $[\Delta c_p/(\gamma_{tot} T_c) = 1.58]$ and of the energy gap ratio $[\Delta(0)/(k_B T_c) = 2.39]$ as well as an exponential decrease of the electronic contribution below $T_c/2$. Together with the saturation of the superfluid density for $T < 3$ K observed by μSR spectroscopy these findings lead us to classify $Sc_5Rh_6Sn_{18}$ as a moderately strong coupled isotropic *s*-wave superconductor. However, above T_c, the crystals reveal a surprisingly anisotropic and large resistivity of 2.5–4.5 mΩ m with metallicalike behavior perpendicular to the *c* axis and by a factor of ∼2 larger parallel to *c*, which decreases upon increasing temperature. These observations are discussed in connection to a characteristic intrinsic disorder in the crystal structure of $Sc_5Rh_6Sn_{18}$.

DOI: 10.1103/PhysRevB.102.024508

I. INTRODUCTION

Unconventional superconductors (SCs) have attracted considerable attention in the solid-state science community in the past few decades. These are materials in which the BCS theory fails to describe the Cooper pairing, which indicates (i) the electron-phonon coupling is not the driving force and (ii) not just the one-dimensional global gauge symmetry U(1) is broken below the transition temperature. In unconventional SCs further symmetries are broken, e.g., time-reversal (TRS) and spatial symmetries [1]. In SCs with broken TRS an internal magnetic field is supported, which is a rare phenomenon of special interest for researchers [2]. Interestingly, superconducting (sc) states obeying TRS are observed for both centrosymmetric (e.g., UPt_3 [3], $PrPt_4Ge_{12}$ [4], $LaNiGa_2$ [5], etc.) and noncentrosymmetric (e.g., $LaNiC_2$ [6], La_7Ir_3 [7], Re_6Ti [8], etc.) compounds. However, for crystal structures without inversion symmetry the parity of the sc wave function has no meaning, and thus, the pairing state cannot be classified as either singlet or triplet [9]. For this reason, TRS breaking seems to be anticipated in noncentrosymmetric SCs.

Superconductivity for $Sc_5Rh_6Sn_{18}$ below the transition temperature $T_c = 4.5$ K was reported for the first time in [10] and later confirmed in [11–13]. Further studies revealed extreme type-II superconductivity with an upper critical magnetic field well below the Pauli limit ($B_{c2} = 7.24$ T) and an enhanced energy gap ratio $[\Delta(0)/(k_B T_c) = 2.65]$. Both these findings indicated an isotropic *s*-wave sc gap with moderately strong electron-phonon coupling [14]. Recently performed zero-field muon-spin rotation (μSR) measurements in longitudinal geometry revealed for $Sc_5Rh_6Sn_{18}$ the spontaneous appearance of an internal magnetic field below T_c. This would imply a breaking of TRS in the sc state and thus unconventional superconductivity with either a singlet $d + id$ state with a line node or, alternatively, nonunitary triplet pairing with point nodes [15].

A highly anisotropic sc gap with point nodes as well as TRS breaking is also reported for the isostructural compound $Y_5Rh_6Sn_{18}$ ($T_c = 3.0$ K, $B_{c2} = 3.1$ T) [16–18], whereas an isotropic *s*-wave gap coexists with a TRS broken state in $Lu_5Rh_6Sn_{18}$ ($T_c = 4.0$ K, $B_{c2} = 6.45$ T) [19]. $Tm_5Rh_6Sn_{18}$ ($T_c = 2.2$ K) is characterized by the coexistence of magnetism and reentrant superconductivity at zero magnetic field [20]. In contrast, conventional BCS superconductivity with an *s*-wave gap is observed for $Sc_5Ru_6Sn_{18}$ ($T_c = 3.5$ K, $B_{c2} = 2.6$ T) [21] and $Sc_5Ir_6Sn_{18}$ ($T_c = 2.64$ K, $B_{c2} = 3.2$ T) [22]. Interestingly, recent field-dependent low-temperature thermal conductivity measurements showed nodeless *s*-wave gaps for both $Y_5Rh_6Sn_{18}$ and $Lu_5Rh_6Sn_{18}$ [23].

Such controversial reports on 5:6:18 stannide SCs as well as our recent combined high-resolution x-ray diffraction and transmission electron microscopy study [24], which indicates locally broken translational symmetry (i.e., the possible

*roman.gumeniuk@physik.tu-freiberg.de

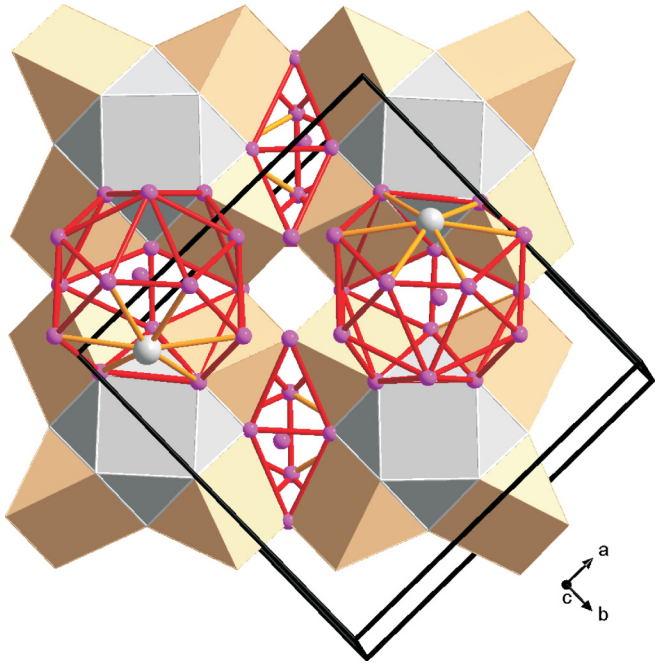

FIG. 1. Array of corner-sharing trigonal prisms (tan) with Rh atoms in the center. Incorporated are Sc1-centered cuboctahedra (gray) and 16-vertex polyhedra composed of Sn atoms and Sc2 with Sn1 in the center.

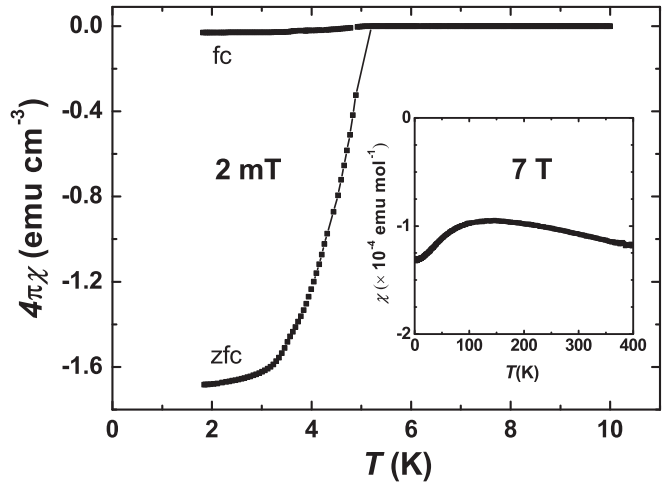

FIG. 2. Magnetic susceptibility ($B = 2$ mT) for $Sc_5Rh_6Sn_{18}$. Inset: magnetic susceptibility for $B = 7$ T measured in ZFC and FC conditions.

presence of microscopic noncentrosymmetric domains) in the complex crystal structure of $Sc_5Rh_6Sn_{18}$ [24], prompted us to perform additional physical property investigations of this compound. In the present work we report on magnetic susceptibility, electrical resistivity, specific heat capacity, and μSR spectroscopy measurements. Muon spectroscopy is a very sensitive local probe for tiny magnetic fields in the bulk of SCs [25] and thus the most appropriate method to detect TRS breaking. Our results indicate that $Sc_5Rh_6Sn_{18}$ is a moderately strong coupled *s*-wave SC without nodes in the gap. Especially, in our sensitive μSR spectroscopy measurements, we find no evidence for a TRS-breaking state, which is actually expected for centrosymmetric crystal structures.

II. EXPERIMENT

The synthesis and complete structural characterization of the octahedral crystals with a base of about 1×1 cm^2 and a height of about 1 cm (see Fig. 1 in [24]), on which the here-reported properties were measured, as well as the electronic structure and chemical bonding of $Sc_5Rh_6Sn_{18}$ are discussed in Ref. [24]. The performed diffraction studies showed $Sc_5Rh_6Sn_{18}$ [space group: $I4_1/acd$, $a = 13.5529(2)$ Å, $c = 27.0976(7)$ Å] crystallizes with the $Sc_5Ir_6Sn_{18}$ type of structure [22]. The structural arrangement can be understood as a corner-sharing trigonal prism array with incorporated cuboctahedra, which are centered by Sc atoms, and 16-vertex polyhedra with the Sn1 atom in the center (Fig. 1).

The magnetization was measured in a superconducting quantum interference device magnetometer (MPMS XL-7, Quantum Design) in external fields between $\mu_0 H = 2$ mT and 7 T and temperatures from 1.8 to 400 K. The electrical resistivity and the heat capacity were measured down to 0.4 K in a commercial system (PPMS-9, Quantum Design) using an ac resistivity bridge (LR-700, Linear Research) and the HC option of the PPMS, respectively. In order to get precise c_p data at the lowest temperatures, the full crystal of ≈ 250-mg mass was measured. The Hall effect was measured in magnetic fields between -9 T and $+9$ T using the ETO option of the PPMS. Electrical contacts were made with silver-filled epoxy glue.

Zero-field (ZF) and transverse field (TF) μSR experiments were performed at the πM3 beamline (Paul Scherrer Institute, PSI Villigen, Switzerland) by using the dedicated GPS spectrometer [26]. In TF experiments, the single crystal of $Sc_5Rh_6Sn_{18}$ depicted in Fig. 1 in Ref. [24] was cooled from above T_c in an applied field of 10 and 50 mT normal to the largest face of the respective crystal. In ZF experiments the Earth's magnetic field was compensated with accuracy better than 30 mG by three orthogonal Helmholtz coils around the spectrometer along the x, y, and z axes [26]. A ^{4}He continuous-flow cryostat allowed measurements above 1.6 K. The typical statistics of measurements for each point were $\approx 18 \times 10^6$ positron events.

III. RESULTS AND DISCUSSION

A. Magnetic susceptibility

Measurements of the high-field magnetic susceptibility showed $Sc_5Rh_6Sn_{18}$ to be diamagnetic in the whole investigated temperature range (inset to Fig. 2), with an extrapolated value of $\chi_0 \approx -136(10) \times 10^{-6}$ emu mol^{-1} at $T = 0$ K. $\chi(T)$ of $Sc_5Rh_6Sn_{18}$ increases with temperature, passes through a broad maximum centered around 150 K, and then decreases. Such a curvature of $\chi(T)$ is rather unexpected, taking into account that both diamagnetic and Pauli paramagnetic susceptibilities are usually temperature independent. A temperature dependence of the Pauli susceptibility can, however, appear due to a steep slope of the DOS near the Fermi level. Such behavior of $\chi(T)$ is documented for

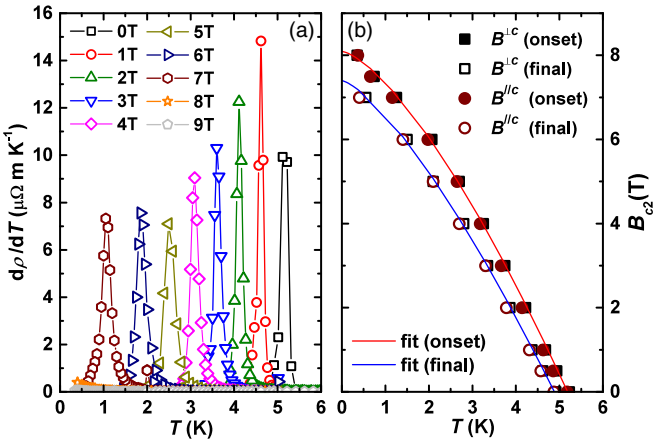

FIG. 3. (a) Resistivity derivatives of $Sc_5Rh_6Sn_{18}$ for current and field parallel to the c axis in magnetic fields up to $B = 9$ T. (b) Upper critical field B_{c2} vs T determined from electrical resistivity data together with fits to a power law (red and blue lines are for onset and zero-resistance (final) points, respectively).

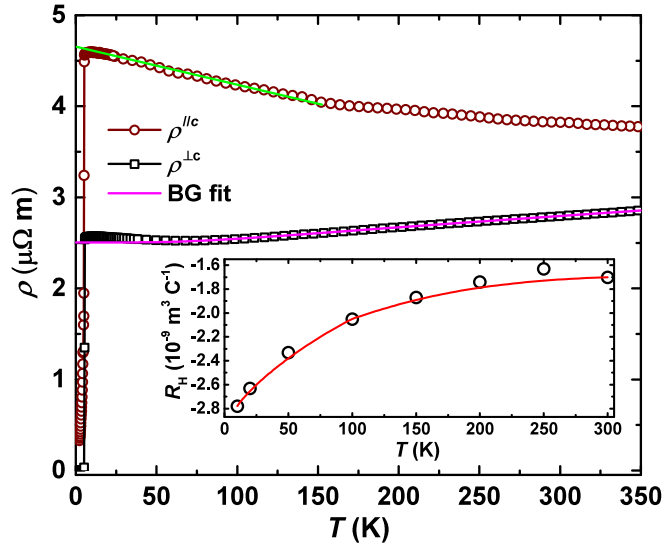

FIG. 4. Electrical resistivity of $Sc_5Rh_6Sn_{18}$ together with Bloch-Grüneisen (purple line) and linear (green line) fits (see text). Inset: Hall coefficient of $Sc_5Rh_6Sn_{18}$. The red line is a guide for the eye.

$BaPt_{4-x}Au_xGe_{12}$ [27]. Figure 5 in Ref. [24] shows that the DOS of $Sc_5Rh_6Sn_{18}$ indeed shows such a steep slope.

The temperature dependence of the zero-field-cooled (ZFC) and field-cooled (FC) magnetic susceptibilities of $Sc_5Rh_6Sn_{18}$ in a field of 2 mT is given in Fig. 2. A sc transition is observed at $T_c^{mag} = 5.2$ K. Considering the demagnetization correction, the diamagnetic response in ZFC is close to complete. The FC signal (Meissner effect) is much weaker, which is most likely due to strong flux line pinning in this type-II superconductor.

B. Electrical transport

The temperature dependence of the electrical resistivity ρ of $Sc_5Rh_6Sn_{18}$ shows a sc transition at $T_c^{res} = 5.2$ K. The derivative of the electrical resistivity measured along the c axis is presented in Fig. 3(a) for different values of $B \parallel c$. The observed transitions are broad (full width at half maximum of 0.2–0.4 K), which is most likely due to structural disorder [24]. An increase of the magnetic field leads to a continuous lowering of T_c, and for $B = 9$ T no indication of superconductivity is observed for temperatures above 0.4 K. Identical behavior of $\rho(T)$ is observed when measuring in a magnetic field perpendicular to the c axis [$B \perp c$; not shown in Fig. 3(a)], indicating no anisotropy of the second critical field.

The field dependence of T_c (defined as the temperature where ρ deviates from zero) for both directions $B \perp c$ and $B \parallel c$ is plotted in Fig. 3(b). Again, a clear isotropic behavior is observed. A power-law extrapolation results in the upper critical field $B_{c2}(0) = 7.75(20)$ T. This corresponds to a Ginzburg-Landau coherence length $\xi_{GL}(0) = 65(1)$ Å, as calculated from $B_{c2} = \Phi_0/2\pi\xi_{GL}^2$ (Φ_0 is the flux quantum $h/2e$). $B_{c2}(0)$ is significantly lower than the Pauli-paramagnetic limit for weak electron-phonon coupling, B_{c2}^p (T) $= 1.86\ T_c$ (K) [28,29].

The electrical resistivity of $Sc_5Rh_6Sn_{18}$ single crystals above the sc transition shows anisotropic behavior (Fig. 4). In directions perpendicular to the c axis, $\rho_{\perp c}$ decreases with decreasing temperature down to 70 K and then slightly increases (almost not visible in Fig. 4), thus showing a broad minimum. The low residual resistivity ratio (RRR $= \rho_{\perp c}^{300K}/\rho_{\perp c}^{6K} = 1.1$) can be explained by the structural disorder reported in [24]. In the temperature range 80–350 K $\rho_{\perp c}$ fits excellently to the Bloch-Grüneisen formula [Eq. (1)], confirming $Sc_5Rh_6Sn_{18}$ is a metallic system with a high residual resistivity due to defect scattering $\rho_{\perp c,0} = 2.50(1)\,\mu\Omega$ m; the coefficient depending on the phonon contribution $A = 0.11(3)\ \mu\Omega$ cm, and Debye temperature $\theta_D^{res}(0) = 460(10)$ K. Here it should be noted that high values of the residual resistivities of about 2.5–4.0 $\mu\Omega$ m as well as a rather weak temperature variation of $\rho(T)$ (RRR ~ 1) were also reported for $Y_5Rh_6Sn_{18}$ and $Lu_5Rh_6Sn_{18}$ crystals in Refs. [17,23]:

$$\rho(T) = \rho_0 + A\left(\frac{T}{\theta_D^{res}}\right)^5 \int_0^{\theta_D^{res}/T} \frac{x^5}{(e^x - 1)(1 - e^{-x})} dx. \quad (1)$$

Interestingly, $\rho_{\parallel c}(T)$ of $Sc_5Rh_6Sn_{18}$ above the SC transition decreases with increasing temperature. This decrease is linear (green line in Fig. 4) in the range 20–150 K with $\rho_{\parallel c,0} = 4.62(3)\,\mu\Omega$ m. Such behavior of the electrical resistivity is reminiscent of those reported for $Y_5Rh_6Sn_{18}$ and $Lu_5Rh_6Sn_{18}$ and is little understood [17,23,30] and may be due to intrinsic structural disorder, as seen in our recent study of the structure of $Sc_5Rh_6Sn_{18}$ [24].

The Hall coefficient $R_H(T)$ for $Sc_5Rh_6Sn_{18}$ is depicted in the inset of Fig. 4. The magnetic field was applied parallel to c, and the electrical current was applied perpendicular. $R_H(T)$ increases with increasing temperature, tends to saturate near room temperature, and is negative in the whole investigated temperature range, which indicates electrons as charge carriers. The charge carrier density $n_e = 2.2$–3.8×10^{27} m^{-3} was calculated within the single-carrier model. Such values are typical for d-metal intermetallic systems [31].

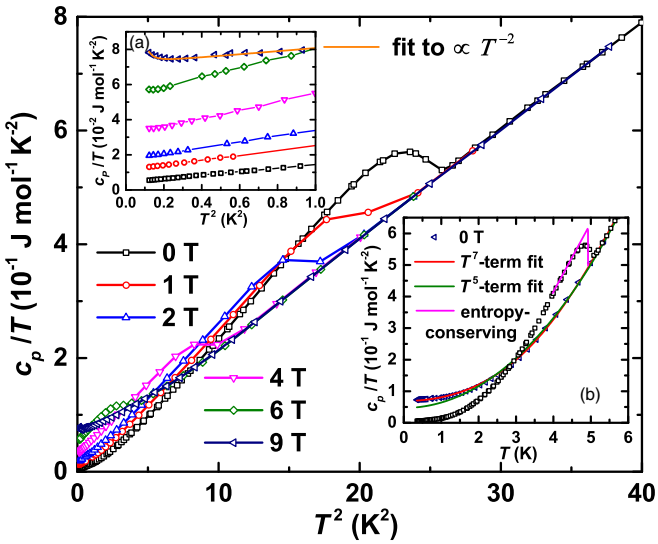

FIG. 5. Specific heat c_p/T vs T^2 for $Sc_5Rh_6Sn_{18}$ in different magnetic fields. Inset a: low-temperature $c_p/T(T^2)$ together with the fit to $\propto T^{-2}$ for $B = 9$ T (see text for more details). Inset b: corrected for the Rh nuclear Schottky anomaly $c_p/T(T)$ in zero and overcritical ($B = 9$ T) magnetic field together with fits including T^5 and T^7 terms as well as a graphical equal-area estimation (entropy conserving; see text).

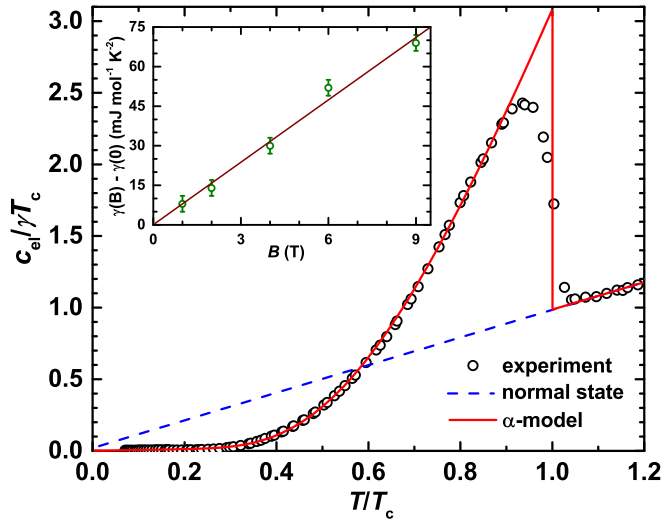

FIG. 6. Electronic specific heat for $Sc_5Rh_6Sn_{18}$ and a comparison with the α model [33]. The nonsuperconducting normal state $c_{el} = \gamma_{tot} T$ is given by the dashed line. Inset: Sommerfeld parameter $\gamma(B)$ as a function of magnetic field B. The solid brown line indicates a linear dependence $\gamma(B) \sim B$ typical for an s-wave gap.

C. Specific heat

The specific heat c_p/T vs T^2 for $Sc_5Rh_6Sn_{18}$ in different magnetic fields is presented in Fig. 5. A sizable but rounded steplike anomaly with an onset $T_c = 5.15$ K (consistent with T_c^{mag} and T_c^{res}) confirms the bulk nature of the superconductivity.

The plot of $c_p/T(T^2)$ of $Sc_5Rh_6Sn_{18}$ reveals a clear upturn for $T < 0.6$ K for magnetic fields $B = 6$ and 9 T [see inset (a) in Fig. 5]. This is probably due to a nuclear Schottky anomaly (i.e., $c_{nucl} \propto T^{-2}$), which is frequently observed in Rh-containing intermetallics [32]. However, even after subtracting this contribution, $c_p(T)$ in the overcritical field could not be described with the conventional ansatz $\gamma T + \beta T^3$. As one can see from inset (b) in Fig. 5, such a fit results in a strongly underestimated Sommerfeld coefficient [$\gamma = 47(2)$ mJ mol^{-1} K^{-2}]. Here it should be noted that the description of the low-temperature phonons is a typical problem of 5:6:18 stannides. To model c_{ph} for $Sc_5Ru_6Sn_{18}$ Kumar *et al.* [21] fitted c_p to $\gamma T + \beta T^3 + \delta T^5$ above $T_c = 3.5$ K. A comparison of the value of $\gamma = 51.1$ mJ mol^{-1} K^{-2} obtained in [15] for $Sc_5Rh_6Sn_{18}$ with Fig. 2(a) in this work hints at its underestimation. For a sufficiently accurate description of $c_{ph}(T)$ of $Sc_5Rh_6Sn_{18}$ in the whole temperature range, it was necessary to include even the T^7 term, i.e., $c_p = \gamma_{tot} T + \beta T^3 + \delta T^5 + \epsilon T^7$. The resulting parameters of such a fit in the temperature range 0.35–6.1 K are the Sommerfeld coefficient of the electronic heat capacity $\gamma_{tot} = 69(1)$ mJ mol^{-1} K^{-2}, $\beta = 11.6(2)$ mJ mol^{-1} K^{-4} (corresponding to $\theta_D^{cal} = 169(1)$ K, which obviously strongly deviates from previously published values [21] due to the inclusion of the additional terms), $\delta = 0.37(2)$ mJ mol^{-1} K^{-6}, and $\varepsilon = -5.3(7)$ μJ mol^{-1} K^{-8}.

The second-order phase transition for zero field was analyzed by a graphical equal-area estimation (entropy conserving) with a midpoint $T_c^{cal} = 4.97$ K [see Fig. 5(b)]. This resulted in the specific heat jump ratio $\Delta c_p/\gamma_{tot} T_c^{cal} = 1.58(3)$, which is slightly larger than that of the weak-coupling BCS-theory limit (i.e., 1.43) for s-wave superconductors.

To obtain the temperature dependence of the electronic specific heat $c_{el}(T)$ we subtracted the phononic contribution c_{ph} from the total c_p. $c_{el}(T)$ in zero field (Fig. 6) is well described within the α model [33] for the energy gap $\alpha \equiv \Delta(0)/k_B T_c = 2.39$ (in fair agreement with Ref. [15]).

The Sommerfeld coefficient $\gamma(B)$ for $Sc_5Rh_6Sn_{18}$ was obtained by fitting $c_p = \gamma T + c_{ph}$ in different magnetic fields with the c_{ph} terms given above. It varies linearly with the magnetic field (inset to Fig. 6). This indicates that $\gamma(B)$ is linearly proportional to the number of field-induced flux lines, indicating an energy gap without nodes. For a strongly anisotropic gap or a gap with nodes $\gamma(B) \propto B^{1/2}$ dependence would be expected.

All these observations are in good agreement with previous reports [14,15] and indicate $Sc_5Rh_6Sn_{18}$ is a superconductor with an isotropic s-wave gap and slightly stronger electron-phonon coupling than predicted by the weak-coupling limit of the BCS theory.

D. Zero-field μSR experiments

ZF-μSR time spectra of $Sc_5Rh_6Sn_{18}$ measured at $T = 2.11$ K and almost at the sc transition temperature ($T = 5.05$ K) are presented in Fig. 7. The raw ZF-μSR data imply that there is almost no (no visible) difference between the T_c and below-T_c data sets. The solid lines in Fig. 7 correspond to the analysis performed by using the following functional form:

$$A^{ZF}(t) = A_0 G_{KT}(t) \exp(-\Lambda t). \quad (2)$$

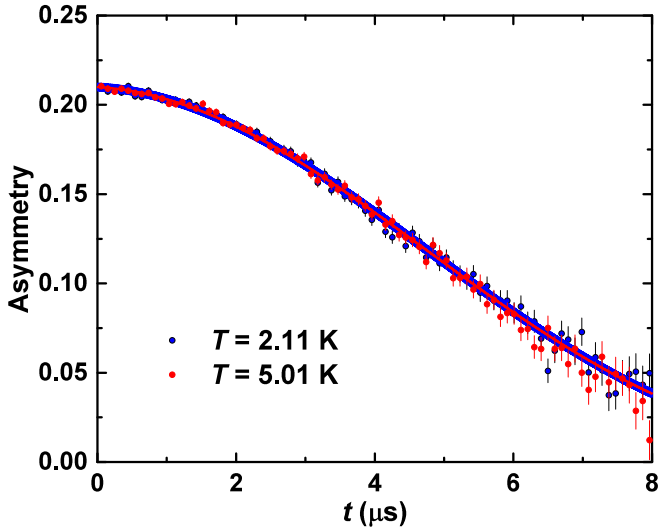

FIG. 7. ZF-μSR time spectra measured at $T = 2.11$ K and near the sc transition temperature ($T = 5.05$ K) in $Sc_5Rh_6Sn_{18}$. The solid lines are fits by using Eq. (2). The absence of a visible difference between the time spectra suggests an absence of the TRS breaking effect (see text for details).

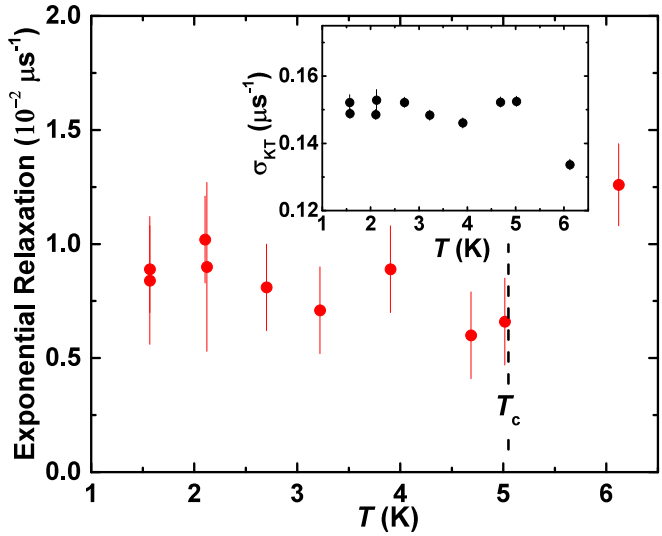

FIG. 9. Temperature dependence of the exponential relaxation rate Λ (main panel) and the Gaussian Kubo-Toyabe relaxation rate σ_{KT} obtained from the fit of ZF-μSR data by means of Eq. (2) (inset). The dashed line denotes $T_c = 5.15$ K.

Here A_0 is the initial muon-spin asymmetry, $G_{KT}(t)$ is the Kubo-Toyabe (KT) relaxation function describing the contribution of nuclear magnetic moments,

$$G_{KT}(t) = \left[\tfrac{1}{3} + \tfrac{2}{3}\left(1 - \sigma_{KT}^2 t^2\right)\exp\left(-\sigma_{KT}^2 t^2/2\right)\right], \quad (3)$$

and Λ is the electronic moment relaxation rate. σ_{KT} is the Gaussian KT relaxation rate.

The temperature dependences of the parameters obtained from the fit of the ZF-μSR data are summarized in Figs. 8 and 9. Two different types of fitting procedures were performed. As a first attempt the relaxation rate σ_{KT} was assumed to be temperature independent. All muon time spectra collected at different temperatures were fitted simultaneously (globally) by using Eq. (2) with A_0 and σ_{KT} being the same and Λ being different for each particular data set. The results presented in Fig. 8 imply that the exponential relaxation rate $\Lambda \simeq 0.01\ \mu s^{-1}$ stays temperature independent up to T_c. More interesting is the fact that the two points, namely, the first one at $T = 5.05$ K, which stays almost exactly at T_c, and the second one at $T = 6.12\ \text{K} > T_c$, demonstrate the steplike change from $\Lambda(T = 5.05\,\text{K}) \simeq 0.011(1)\ \mu s^{-1}$ to $\Lambda(T = 6.12\,\text{K}) \simeq 0.0\ \mu s^{-1}$.

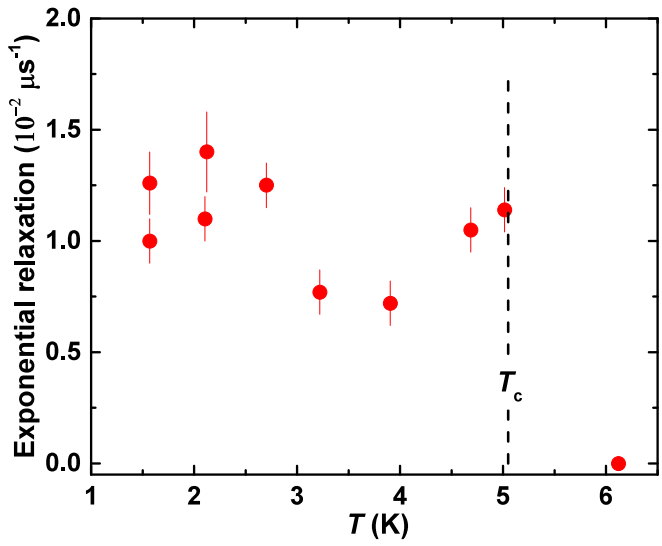

FIG. 8. Temperature dependence of the exponential relaxation rate Λ obtained from the fit of ZF-μSR data by means of Eq. (2). The Gaussian Kubo-Toyabe relaxation rate σ_{KT} was assumed to be temperature independent. The dotted line denotes the sc transition temperature $T_c = 5.15$ K.

As the second attempt, the validity of the assumption about the temperature-independent Gaussian KT relaxation rate σ_{KT} was checked. The results of the "global" fit procedure with both Λ and σ_{KT} assumed to be temperature dependent are presented in Fig. 9. The analysis reveals the whole effect of the sudden change of the relaxation rate at $T = 6.12$ K went entirely to σ_{KT}, while Λ stays almost temperature independent within the experimental uncertainty.

Importantly, Bhattacharyya *et al.* [15] recently reported the appearance of spontaneous magnetic fields in ZF-μSR data in $Sc_5Rh_6Sn_{18}$. This allowed them to make a conclusion on the existence of the TRS-breaking phenomena and point to an unconventional pairing mechanism in $Sc_5Rh_6Sn_{18}$. Our data, however, cannot be reconciled with the observation of Bhattacharyya *et al.* [15] for the following reasons:

(i) The maximum value of the exponential rate Λ observed in our study ($\Lambda \simeq 0.010\ \mu s^{-1}$) is at least two times smaller than $\Lambda \simeq 0.021\ \mu s^{-1}$ reported in Ref. [15] (see Figs. 8 and 9). This suggests that the value of the spontaneous magnetic field on the muon stopping position caused by the effect of the TRS breaking is *sample dependent*, which cannot be the case.

(ii) Analysis with the Gaussian KT relaxation as a temperature-dependent parameter shows that the tiny

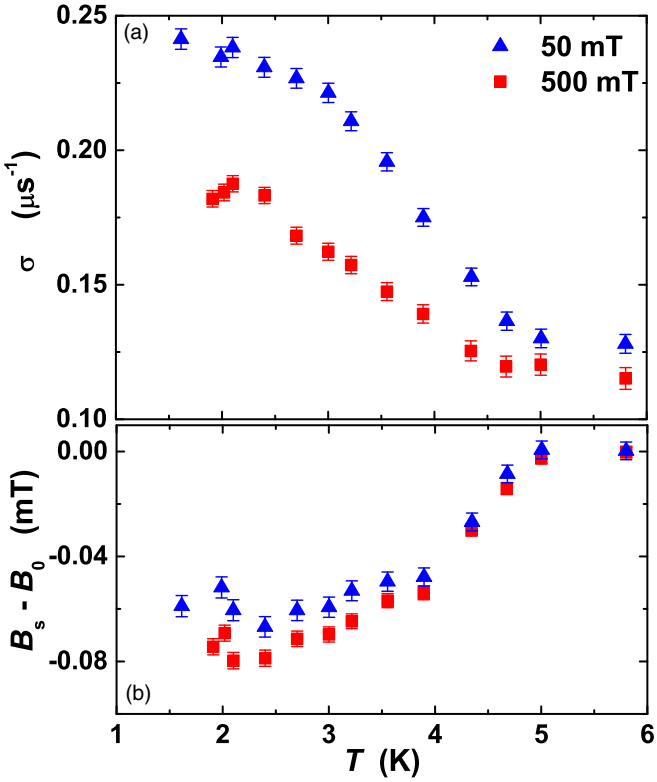

FIG. 10. Temperature dependence of (a) σ and (b) $B_s - B_0$ in $Sc_5Rh_6Sn_{18}$ obtained by fitting TF μSR time spectra with Eq. (4). Here B_0 is the mean field of the sample above T_c.

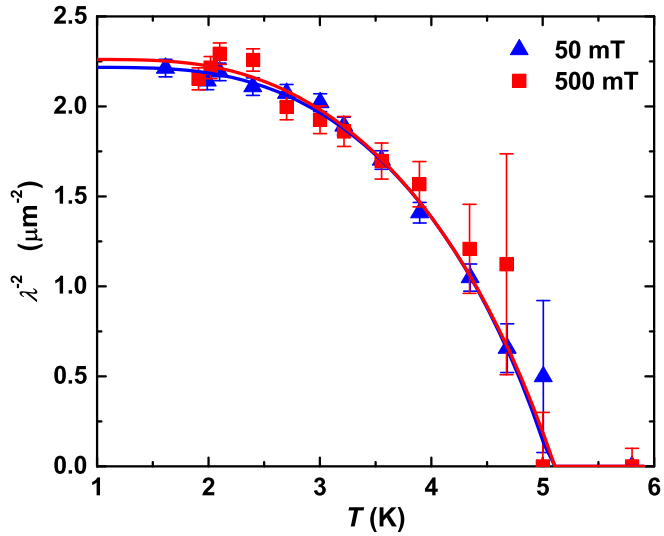

FIG. 11. Temperature dependence of λ^{-2} in $Sc_5Rh_6Sn_{18}$ calculated from σ_s as is obtained by fitting TF μSR time spectra with Eq. (4).

difference in relaxation is caused by the change in σ_{KT} rather than the exponential relaxation parameter (Fig. 9).

(iii) Even though the inaccuracy in the determination of Λ in our studies is higher than that reported in Ref. [15], no systematic decrease of Λ occurred when approaching T_c from low temperatures. In contrast to the observation of Bhattacharyya *et al.* [15], in our experiments Λ remains constant all the way up to T_c.

To conclude, our ZF-μSR experiments do not confirm the appearance of the time-reversal symmetry-breaking phenomena in $Sc_5Rh_6Sn_{18}$.

E. Transverse-field μSR experiments

In the transverse-field μSR the external magnetic field is applied perpendicular to the initial muon-spin polarization. In sc materials the TF muon-spin depolarization above T_c is dominated by the temperature-independent nuclear depolarization σ_n. Below T_c an additional depolarization σ_s takes place due to the spatially inhomogeneous magnetic field of the Abrikosov vortex lattice [34]. The experimental TF-μSR data were analyzed by using the following functional form:

$$A^{TF}(t) = A_0 \exp\left[-\left(\sigma_s^2 + \sigma_n^2\right)t^2/2\right]\cos(\gamma_\mu B_s t + \phi). \quad (4)$$

Here B_s is the internal field at the muon-stopping position, $\gamma_\mu = 2\pi \times 135.52$ MHz/T is the muon gyromagnetic ratio, and ϕ is the initial phase of the muon-spin ensemble.

In Fig. 10 temperature dependences of $\sigma = \sqrt{\sigma_s^2 + \sigma_n^2}$ and B_s in $Sc_5Rh_6Sn_{18}$ for applied fields of 50 and 500 mT are shown. Above T_c a nuclear depolarization of $\sigma_n = 0.127(2)\ \mu s^{-1}$ is observed, while below $T_c = 5.15$ K σ increases and reaches a value of $0.240(2)\ \mu s^{-1}$ in the low-temperature limit. The field in the sample below T_c decreases due to diamagnetism in the sc state.

The temperature dependence of the magnetic penetration depth λ is related to the temperature dependence of the muon relaxation rate due to the Abrikosov vortex lattice σ_s through the relation [35]

$$\sigma_s(b)(\mu s^{-1}) = 4.83 \times 10^4(1-b) \times [1 + 1.21(1-\sqrt{b})^3]\lambda^{-2}(nm^{-2}), \quad (5)$$

where $b = B_s/B_{c2}(T)$ is the reduced field, with B_{c2} denoting the upper critical field.

The superfluid density is an important parameter characterizing a superconductor and is proportional to λ^{-2} [36]. The temperature dependence of λ^{-2} is shown in Fig. 11. In the low-T limit $Sc_5Rh_6Sn_{18}$ shows a saturation of the superfluid density, indicating a nodeless sc order parameter, in agreement with the exponential decrease of the electronic specific heat. Within our precision, no field dependence of the magnetic penetration depth is observed, thus indicating an *s*-wave sc order parameter. Consequently, we analyze the temperature dependence of λ^{-2} within the clean-limit *s*-wave BCS model [37],

$$\frac{\lambda^2(0)}{\lambda^2(T)} = 1 + 2\int_{\Delta(T)}^{\infty}\left(\frac{\partial f}{\partial E}\right)\frac{EdE}{\sqrt{E^2 - \Delta^2(T)}}, \quad (6)$$

where $f = [1 + \exp(E/k_BT)]^{-1}$ is the Fermi function, while the temperature dependence of the BCS gap is obtained with the equation $\Delta(T) = \Delta_0 \tanh\{1.82[1.018(1/t - 1)]^{0.51}\}$, with $t = T/T_c$ [38,39]. A fit of Eq. (6) to the data is shown in Fig. 11. The BCS model describes the data quite well. The results of the analysis are summarized in Table I. The $\lambda(0)$ values are, by a factor of ≈ 2, larger than those reported in [15]. Taking into account that μSR is the most reliable

TABLE I. Summary of fit parameters for $\lambda^{-2}(T)$ using Eq. (6).

B_{ext} (mT)	$\lambda(0)$ (nm)	Δ (meV)	$\Delta(0)/k_BT_c$
50	672(6)	1.07(4)	2.46(9)
500	665(8)	1.04(7)	2.38(16)

technique to estimate $\lambda(0)$, our precise data clearly support a nodeless *s*-wave scenario.

From the coherence length and penetration depth we determined the Ginzburg-Landau parameter $\kappa = \lambda/\xi = 103$, which allows us to classify $Sc_5Rh_6Sn_{18}$ as an extreme type-II superconductor.

IV. CONCLUSIONS

$Sc_5Rh_6Sn_{18}$ is a diamagnetic metallic compound with a complex centrosymmetric tetragonal crystal structure and a high degree of structural disorder [24]. On a local scale the disorder is expected to induce deviations from the global centrosymmetric structure of the crystal [24]. $Sc_5Rh_6Sn_{18}$ reveals a relatively broad sc transition at $T_c = 5.15$ K. The upper critical field $B_{c2} = 7.75$ T is well below the Pauli limit and is the same perpendicular and parallel to the *c* direction. Both the specific heat jump $\Delta c_p/(\gamma_{tot}T_c) = 1.58$ and energy gap ratio $\Delta(0)/k_BT_c = 2.39$ for $Sc_5Rh_6Sn_{18}$ are larger than the values for the BCS weak-coupling limit of 1.43 and 1.76, respectively. These findings together with the exponential decrease of the electronic specific heat below $T_c/2$ indicate the studied stannide is an *s*-wave superconductor with electron-phonon coupling slightly stronger than the weak-coupling BCS limit. This conclusion is strongly substantiated by the observed saturation of the superfluid density at low temperature as well as the absence of time-reversal symmetry breaking, both deduced from precise muon-spin rotation. Although $Sc_5Rh_6Sn_{18}$ has a large Ginzburg-Landau parameter (extreme type-II superconductivity), the coherence length of ≈ 65 Å is still much longer than the typical length scale of the structural disorder [24]. It might be speculated that for this reason the local deviations from the global centrosymmetric structure imposed by the structural defects do not critically influence the symmetry of the sc order parameter.

The electrical resistivity reveals anisotropic behavior above the sc transition: $\rho_{\perp c}(T)$ increases with increasing temperature, whereas $\rho_{\parallel c}(T)$ is, by a factor of $\sim$2, higher and almost linearly decreases with temperature. The relatively high electrical resistivity in both directions in the $Sc_5Rh_6Sn_{18}$ single crystals is ascribed to the high level of intrinsic structural disorder [24] in $Sc_5Rh_6Sn_{18}$.

ACKNOWLEDGMENTS

This work is performed within DFG (Deutsche Forschungsgemeinschaft) Grant No. 325295543. The authors thank J. Chang for his contribution in the initial phase of this project. This work was partly performed at the Swiss Muon Source (SμS), Paul Scherrer Institut (PSI), Switzerland. A.M. and L.H. acknowledge support by the Swiss National Science Foundation and the NCCR Program MaNEP.

[1] G. R. Stewart, Adv. Phys. **66**, 75 (2017).
[2] M. Håkansson, T. Löfwander, and M. Fogelström, Nat. Phys. **11**, 755 (2015).
[3] G. M. Luke, A. Keren, L. P. Le, W. D. Wu, Y. J. Uemura, D. A. Bonn, L. Taillefer, and J. D. Garrett, Phys. Rev. Lett. **71**, 1466 (1993).
[4] A. Maisuradze, W. Schnelle, R. Khasanov, R. Gumeniuk, M. Nicklas, H. Rosner, A. Leithe-Jasper, Y. Grin, A. Amato, and P. Thalmeier, Phys. Rev. B **82**, 024524 (2010).
[5] A. D. Hillier, J. Quintanilla, B. Mazidian, J. F. Annett, and R. Cywinski, Phys. Rev. Lett. **109**, 097001 (2012).
[6] J. Quintanilla, A. D. Hillier, J. F. Annett, and R. Cywinski, Phys. Rev. B **82**, 174511 (2010).
[7] J. A. T. Barker, D. Singh, A. Thamizhavel, A. D. Hillier, M. R. Lees, G. Balakrishnan, D. M. Paul, and R. P. Singh, Phys. Rev. Lett. **115**, 267001 (2015).
[8] D. Singh, S. K. P., J. A. T. Barker, D. M. Paul, A. D. Hillier, and R. P. Singh, Phys. Rev. B **97**, 100505(R) (2018).
[9] *Non-centrosymmetric Superconductors*, edited by E. Bauer and M. Sigrist (Springer, Berlin, 2012).
[10] J. Remeika, G. Espinosa, A. Cooper, H. Barz, J. Rowell, D. McWhan, J. Vandenberg, D. Moncton, Z. Fisk, L. Woolf *et al.*, Solid State Commun. **34**, 923 (1980).
[11] G. Espinosa, Mater. Res. Bull. **15**, 791 (1980).
[12] G. Espinosa, A. Cooper, and H. Barz, Mater. Res. Bull. **17**, 963 (1982).
[13] G. Venturini, M. Kamta, E. M. Rae, J. Marêchè, B. Malaman, and B. Roques, Mater. Res. Bull. **21**, 1203 (1986).
[14] N. Kase, S. Kittaka, T. Sakakibara, and J. Akimitsu, J. Phys. Soc. Jpn. **81**, SB016 (2012).
[15] A. Bhattacharyya, D. T. Adroja, N. Kase, A. D. Hillier, A. M. Strydom, and J. Akimitsu, Phys. Rev. B **98**, 024511 (2018).
[16] N. Kase, K. Inoue, H. Hayamizu, and J. Akimitsu, J. Phys. Soc. Jpn. **80SA**, SA112 (2011).
[17] N. Kase, S. Kittaka, T. Sakakibara, and J. Akimitsu, JPS Conf. Proc. **3**, 015042 (2014).
[18] A. Bhattacharyya, D. Adroja, N. Kase, A. Hillier, J. Akimitsu, and A. Strydom, Sci. Rep. **5**, 12926 (2015).
[19] A. Bhattacharyya, D. T. Adroja, J. Quintanilla, A. D. Hillier, N. Kase, A. M. Strydom, and J. Akimitsu, Phys. Rev. B **91**, 060503(R) (2015).
[20] N. Kase, J. Akimitsu, Y. Ishii, T. Suzuki, I. Watanabe, M. Miyazaki, M. Hiraishi, S. Takeshita, and R. Kadono, J. Phys. Soc. Jpn. **78**, 073708 (2009).
[21] D. Kumar, C. N. Kuo, F. Astuti, T. Shang, M. K. Lee, C. S. Lue, I. Watanabe, J. A. T. Barker, T. Shiroka, and L. J. Chang, J. Phys.: Condens. Matter **30**, 315803 (2018).
[22] V. Levytskyi, M. Feig, L. Akselrud, W. Schnelle, A. Leithe-Jasper, V. Dyadkin, D. Chernyshov, and R. Gumeniuk, J. Phys.: Condens. Matter **31**, 445603 (2019).

[23] Z. Zhang, Y. Xu, C. N. Kuo, X. C. Hong, M. X. Wang, P. L. Cai, J. K. Dong, C. S. Lue, and S. Y. Li, Supercond. Sci. Technol. **28**, 105008 (2015).
[24] M. Feig, L. Akselrud, W. Schnelle, V. Dyadkin, D. Chernyshov, A. Ormeci, P. Simon, A. Leithe-Jasper, and R. Gumeniuk, Dalton Trans. **49**, 6832 (2020).
[25] A. Amato, Rev. Mod. Phys. **69**, 1119 (1997).
[26] A. Amato, H. Luetkens, K. Sedlak, A. Stoykov, R. Scheuermann, M. Elender, A. Raselli, and D. Graf, Rev. Sci. Instrum. **88**, 093301 (2017).
[27] R. Gumeniuk, H. Rosner, W. Schnelle, M. Nicklas, A. Leithe-Jasper, and Y. Grin, Phys. Rev. B **78**, 052504 (2008).
[28] A. M. Clogston, Phys. Rev. Lett. **9**, 226 (1962).
[29] B. S. Chandrasekhar, J. Appl. Phys. Lett. **1**, 7 (1962).
[30] N. Ali and W. Datars, J. Less-Common Met. **127**, 49 (1987).
[31] R. Groos and A. Marx, *Festkörperphysik* (Oldenbourg, Munich, 2012).
[32] A. Steppke, M. Brando, N. Oeschler, C. Krellner, C. Geibel, and F. Steglich, Phys. Status Solidi B **247**, 737 (2010).
[33] D. Johnston, Supercond. Sci. Technol. **26**, 115011 (2013).
[34] A. Abrikosov, Sov. Phys. JETP **5**, 1174 (1957).
[35] E. H. Brandt, Phys. Rev. B **68**, 054506 (2003).
[36] J. E. Sonier, J. H. Brewer, and R. F. Kiefl, Rev. Mod. Phys. **72**, 769 (2000).
[37] M. Tinkham, *Introduction to Superconductivity* (McGraw-Hill, New York, 1996).
[38] A. Carrington and F. Manzano, Physica C (Amsterdam, Neth.) **385**, 205 (2003).
[39] A. Maisuradze, M. Nicklas, R. Gumeniuk, C. Baines, W. Schnelle, H. Rosner, A. Leithe-Jasper, Y. Grin, and R. Khasanov, Phys. Rev. Lett. **103**, 147002 (2009).